Fusion Engineering and Design 216 (2025) 115088

Contents lists available at ScienceDirect

Fusion Engineering and Design

journal homepage: www.elsevier.com/locate/fusengdes

Thermo-structural analysis on the DTT ECH Transmission Line Single-Beam mirrors

A. Salvitti [a,*], A. Moro [b], A. Bruschi [b], G. Calabrò [a], F. Fanale [b], P. Fanelli [a], S. Garavaglia [b], G. Granucci [b,c], S. Meloni [a], P. Platania [b], A. Romano [c,d]

[a] Department of Economics, Engineering, Society and Business Organization (DEIM), University of Tuscia, Largo dell'Università, Viterbo, 01100, Italy
[b] Institute for Plasma Science and Technology, National Research Council (ISTP-CNR), Via Cozzi 53, 20125 Milan, Italy
[c] DTT S.C.a r.l., Via E. Fermi 45, I-00044, Frascati, (RM), Italy
[d] ENEA, Fusion and Nuclear Safety Department, C.R. Frascati, Via E. Fermi 45, 00044 Frascati, (RM), Italy

ARTICLE INFO

Keywords:
ECH
SBTL
Mirror
Thermal-structural analysis
Temperature
Deformation

ABSTRACT

The Electron Cyclotron Heating (ECH) of the Divertor Tokamak Test (DTT) facility is its main system to heat the plasma with an installed power of 32 MW. A cluster of the ECH consists of 1 MW/170 GHz sources (8 gyrotrons), a quasi-optical Transmission Line (TL) and two antennas. The TL efficiently transmits the microwave beams, produced by gyrotrons, up to the launchers. Based on the quasi-optical concept, the TL employs mirrors for the transmission of the beams. One of the three segments in which it is conceptually divided is a Single-Beam section in the Gyrotron hall (SBG), where the beams propagate with an independent optical path. A small fraction of beam power is absorbed by the reflecting mirror due to ohmic losses, resulting in a total power absorbed by an SBG mirror of ~1-2 kW. The mirror temperature increases, generating deformations. The loss of the nominal shape of the mirror can contribute to reducing the transmission efficiency, compromising the nominal parameters that ensure the effective performance of the beam propagation system. The conceptual design of different SBG mirrors is carried out, simulating the thermal-structural behaviour. The mirrors, actively water-cooled through channels designed as elongated spirals with variable pitch, achieve maximum temperatures of 28 °C and low deformations (~23 μm), demonstrating the effectiveness of the cooling system. In the end, the same method is then applied in a parametric analysis of the thickness to evaluate the best performance, if necessary. It showed that the initial assumption on the thickness appears to be a well-founded choice.

1. Introduction

The Divertor Tokamak Test (DTT) facility, under construction in Frascati (Italy), has the aim to study alternative power-exhaust solutions [1]. To operate under integrated physics and technical conditions relevant to the exploitation of the future DEMO reactor [2], 45 MW of auxiliary power to the plasma is foreseen to be provided by external heating systems. The main system covering this requirement (~29 MW) is the Electron Cyclotron Heating (ECH) [3–6]. The ECH total power will be guaranteed by 4 clusters, where each one consists of three main parts: 1 MW/170 GHz sources (8 gyrotrons), a Transmission Line (TL) [7–9] and two launching antennas [10]. In DTT, the gyrotrons are located in a specific building, external to the tokamak ("ECH building", the gyrotrons hall). They generate microwave beams with a power of 1 MW at 170 GHz for 100 s. Such beams are transmitted to the plasma, through an evacuated TL, based on quasi-optical propagation of Gaussian beams [11,12] as that one of W7-X [13], but under vacuum. The TL runs over a bridge (also known as the "ECH corridor") from the ECH building to the tokamak hall where, instead, the launchers are. The TL is conceptually divided into three main segments: a Single-Beam section in the Gyrotron hall (SBG), where the beams from the gyrotrons propagate with an independent optical path, a Multi-Beam (MB) section where the eight beams of a given cluster are grouped in a single optical path (in the corridor) and a final Single-Beam section where the bundle of eight beams is split into independent optical paths towards the dedicated DTT sectors hosting the ECH launchers (SBD) [7–9]. The basic element of the propagation is a mirror, in configuration focusing or flat, depending on its function in a confocal arrangement [1,3–9].

One of the main objectives in the TL design is to ensure a minimum transmission efficiency of 90 % in terms of power to the plasma. The

* Corresponding author.
E-mail address: alessandra.salvitti@unitus.it (A. Salvitti).

https://doi.org/10.1016/j.fusengdes.2025.115088
Received 14 December 2024; Received in revised form 7 March 2025; Accepted 11 April 2025
Available online 23 April 2025

propagation is subject to unavoidable losses due to the degradation of the beam quality [9]. In particular, during the reflection on the mirror, due to ohmic losses, a small fraction of the beam power is absorbed by the mirror, losing part of the beam power (first one), furthermore, the mirror heats up, generating deformations due to thermal expansion, and so, losing the original shape for the best reflection (second one). The change of the features of the nominal design leads to inefficiency and this is the main concept driving the mirror design. To preserve the mirrors, they are actively cooled with water, reducing temperature and deformations. The more efficient the cooling circuit is, the less the mirror will deform.

In the papers [14–15], details of the activities related to the design of the MB mirrors, beginning with the selection of an optimal solution among various configurations [14], and progressing to a comprehensive analysis of all MB mirror configurations [15] are given. This analysis was crucial for reconstructing the deformed reflective surfaces and evaluating the total losses. This work aims to complete the evaluation of losses by providing a comprehensive framework that also includes other types of mirrors in the line, focusing on the SB mirrors, starting with the SBG mirrors. The conceptual design of various water-cooled SBG mirrors is developed, with simulations conducted to assess their thermal-structural behaviour. This approach is subsequently applied to a parametric thickness analysis to determine the optimal performance, if required.

2. SBG mirrors

The SBG mirrors are the first mirrors guiding the beams from the source towards the combiner unit (CU), where they are bundled to be transmitted in the MBTL. Fig. 1 shows the first path of a single beam, that from a specific Gyrotron (G) reaches the CU. The beams far from the centre follow the Long-Line (L), instead the beams near the centre follow the Short-Line (S). So, the beam of the L-Line reflects on the mirror 01M-L in the first column (green) and then on the mirrors 02M-L and 03M-L in the second column (pink). The beams of the S-Line reflect only on the mirrors 01M-S and 02M-S, both in the second column.

In the present paper, four mirrors are considered, as main models representing all the SBG mirrors: three mirrors of the L-Line 01M-L, 02M-L and 03M-L (respectively focusing, flat and focusing) and one mirror of the S-Line 02M-S (focusing).

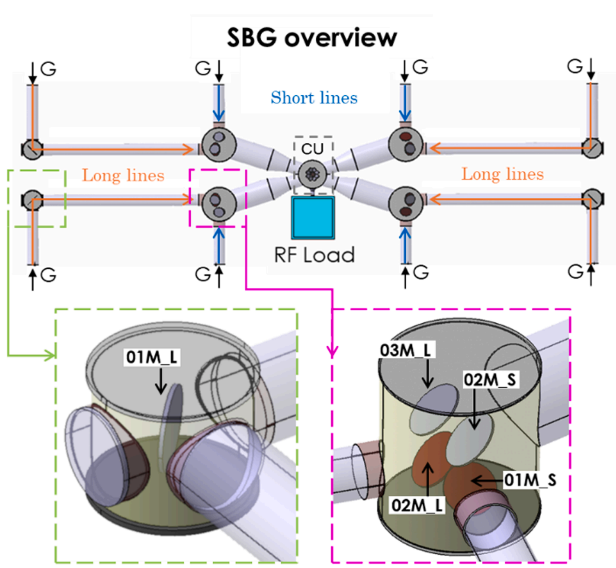

Fig. 1. Overview of the Single Beam mirrors Gyrotron side.

2.1. Models

The basic shape of the SBG mirrors is elliptical with dimensions reported in Table 1. The focusing surface of the three mirrors is a portion of an ellipsoid of revolution. Fig. 2 reports the geometrical data to define the surface, representing a 45° mirror with normal $\hat{n}$. The rays r1 and r2 indicate the distances between the centre of the surface and the focal points: r1 is the reference for the 1st focus (F1) along the axis of the incident beam, whilst r2 is for the 2nd focus (F2) along the axis of the reflected beam.

The elliptical mirror is designed on the origin of the global reference system tilted at 45° (Fig. 3). The ellipsoid is then generated based on a 2D ellipse. By definition, the ellipse's major semi-axis is given by $a = \frac{r1+r2}{2}$. The major axis is on the line joining the focal points, with the ellipse's centre positioned at the midpoint of the segment F1-F2. The ellipse is constructed by constraining the centre, distance 'a', and designating the origin of the mirror as a transition point. The lengths 'b' and 'c' (in grey in Fig. 3) are derived because they depend on the other parameters.

The model of each mirror consists of a bulk with a thickness of 18 mm and a top layer with a minimum thickness in the centre of 2 mm, both made of pure Copper (Cu) (Fig. 4).

About the material, it is worth noting that the results presented in the following sections of the paper are easily extended to a model with the bulk in Cu-alloy (CuCrZr) and the layer in Cu. The copper alloy closely resembles pure copper in many physical properties: at 20 °C, both share the same thermal expansion coefficient, although the alloy exhibits approximately 20 % lower thermal conductivity. So, from a thermal point of view, the alloy should lead to a slightly higher temperature. A preliminary analysis conducted on a SB mirror showed that the percentage difference in the maximum temperature and maximum total deformation is ~1 %.

The cooling channel, in the bulk, features an elongated spiral shape. The concept is the same used in the papers [14–15,17–19], but now, the novelty is the variable pitch of the spiral, which allows it to be denser at the centre. This design enhances cooling efficiency in the area where the heat flux is concentrated, in the current case of a single beam. The inlet is in proximity to the centre and the outlet is at the edge of the minor axis. The spiral parametric Eq. (1) is reported below and visible in Fig. 5:

$$\begin{cases} x = \left(\frac{r_{major}}{r_{minor}}\right)\cdot\frac{0.04(\theta-\pi)+7}{2\pi}\cdot\theta\cdot sin(\theta)\ [mm] \\ y = \frac{10}{2\pi}\cdot\theta\cdot cos(\theta)\ [mm] \\ \pi\ rad < \theta < 23\pi\ rad \end{cases} \tag{1}$$

The spiral pitch on the y-axis is 10 mm constant, instead, the pitch on the x-axis is amplified with the ratio of radii and linearly variable in θ. The cross-section of the channel is semi-circular, with a radius of 3.5 mm (Fig. 5).

2.2. Thermal load

The Single-Beam Mirrors (SBMs) are dedicated to the reflection of a single beam. The thermal load on the mirror comes from the absorbed fraction of the power transported by the beam, featured with Gaussian distribution, as defined in the papers [14–15]. The total power of the

Table 1
Geometrical data of the SBG mirrors.

Mirror model	**Major radius**	**Minor radius**	**Focusing rays r1/r2 [mm/mm]**
01 M L-Line	177 mm	125 mm	1857/14955
02 M L-Line	172 mm	122 mm	FLAT
03 M L-Line	175.5 mm	124 mm	15470/3082
02 M S-Line	178 mm	126 mm	1865/3115

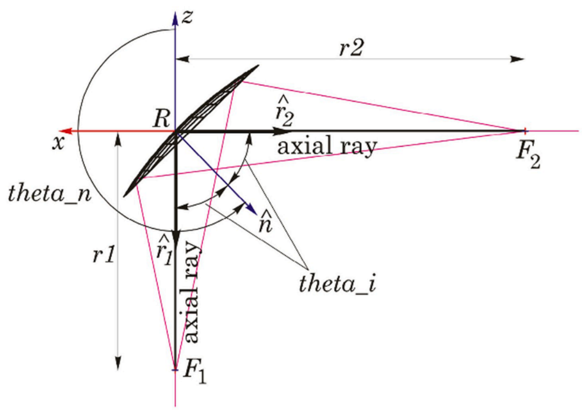

Fig. 2. Reference for elliptical focusing surface [16].

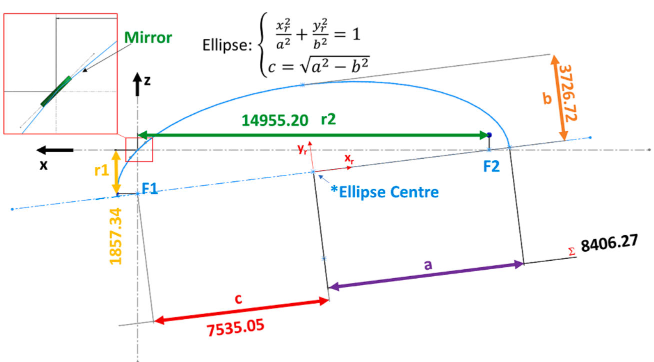

Fig. 3. Definition of the elliptical reflecting surface for the mirror 01M-L.

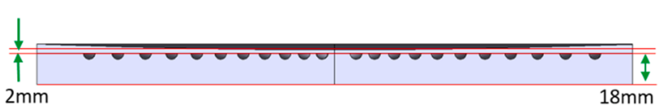

Fig. 4. Section view on the z-x plane of the mirror 01M-L.

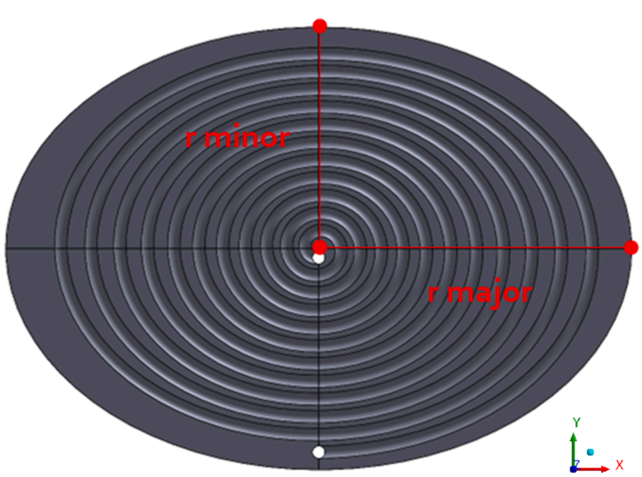

Fig. 5. Front view of the dug bulk of the mirror 01M-L.

beam is $Q = 1$ MW. The projected beam widths along the x and y mirror directions and the absorption coefficients are reported in Table 2. The total absorbed power varies in the range of 1.1–2.1 kW, depending on the different loads, caused by the different angle between polarization and incidence planes on the various mirrors. The maximum power

Table 2
Microwave load parameters.

Mirror Model	w_x [mm]	w_y [mm]	A	$P_{abs\ MAX}$ [W/m^2]
01 M L-Line	88.59	62.64	0.21 %	240910
02 M L-Line	86.08	60.87	0.11 %	133650
03 M L-Line	87.81	62.09	0.11 %	128440
02 M S-Line	88.97	62.91	0.20 %	227480

concerns the mirror 01M-L due to the highest absorption coefficient, also visible from the peak value of the total absorbed heat flux in the last column of Table 2. Fig. 6 shows the heat flux distribution of the mirror 01M-L.

3. Finite element models

The realization of the mesh models required high refinement grade. Because of the very small deformations expected for these mirrors, very fine meshes are necessary to ensure consistency and accuracy of the results. They are realized in ANSA software [20], predominantly structured, as depicted in Fig. 7, with an average of $2.48 \cdot 10^6$ elements and $2.51 \cdot 10^6$ nodes. Linear elements, mainly hexahedrons, were used. The average skewness has a value of 0.16, confirming the high quality of the mesh.

Thermal and structural finite-element analyses were performed with ANSYS software. The methodology applied in the thermal analysis, with the employment of the thermal-flow element FLUID116, is discussed in other papers [14–15,21]. It is used to simulate also fluid behaviour, mass and heat transport, and convection effects, but without other fluid-dynamics features. For these mirrors, computational fluid dynamics (CFD) analyses are not planned. A comparison between the applied methodology and CFD was previously conducted on a mirror presented in [22], showing no significant differences in the thermal load distribution. Furthermore, in cases where only thermal analysis was performed, the values obtained are in a conservative range (maximum temperature discrepancy lower than 4 %). Taking into account the aforementioned analyses, since the mirrors and thermal conditions of this paper closely resemble those in [22], the thermal results will be considered reliable at this stage of the design.

The convection Heat Transfer Coefficient (HTC) is calculated using the Dittus-Boelter equation and is assumed to remain constant due to the low-temperature gradients involved.

Because of the high level of mesh refinement, transient analyses are computationally intensive. To optimize resource usage, an initial transient analysis is conducted to assess whether a less demanding approach is viable. If this initial analysis confirms that transient studies are

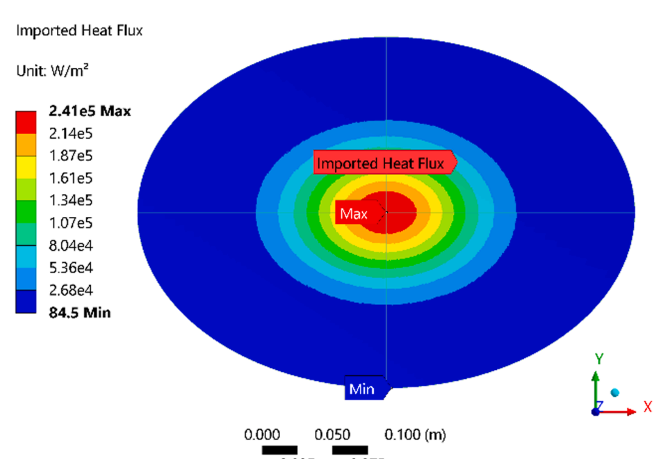

Fig. 6. Contour plot of the heat flux distribution for the microwave load on Mirror 01M-L.

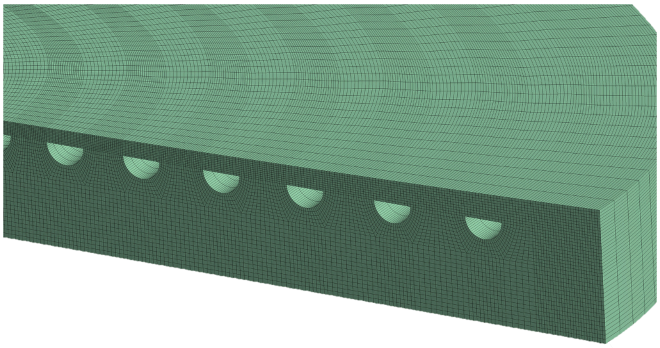

Fig. 7. Mesh model of the 01M-L mirror: detail of the section view on the z-x plane.

unnecessary, each mirror is subsequently evaluated through steady-state thermal and static structural simulations. The transient analysis is performed over 150 s, in which cooling is always active, while heat flux is active between 10 s and 110 s, simulating beam reflection.

The SBMs share the cooling line with the MB mirrors, so, the inlet temperature is the same as [15]. Instead, the lower power to be disposed of permits to decrease in the volume flow rate, as for the smaller mirrors of the launcher [21,22], comparable with the SBMs in size.

The input parameters of the thermal analysis are:

- water inlet temperature $T_{water\ (inlet)} = 15\ ^{\circ}C$,
- water inlet pressure: $p_{water\ (inlet)} = 8\ bar$ (according to DTT water cooling system),
- volumetric flow rate: $\dot{V} = 4.2\ L/min$,
- heat transfer coefficient: $HTC \approx 15000\ W/(m^2K)$, constant, calculated considering the water properties at $T_{water_{inlet}}$.

For the considered volumetric flow rate the average fluid velocity is 3.6 m/s (similar to [22], where peak values reached 6 m/s). The relatively low velocity and the expected lower velocity near the walls do not indicate a significant corrosion risk for copper at this stage of the work. However, this aspect will be further investigated in future developments.

The boundary conditions of the structural analysis are:

- the temperature distribution,
- the water pressure on the channel walls (maintained conservatively constant at 8 bar),
- the forces at the inlet and the outlet that simulate the continuity of the flow, calculated as $F = p{\cdot}S$, where S is the section of the inlet and outlet. The total value of the single force is: ~31 N.

The constraint is a small fixed support in the centre of the back surface, leaving the mirror as free as possible to deform in any direction, to better appreciate the main effect of the temperature, regardless of any constraints (Fig. 8).

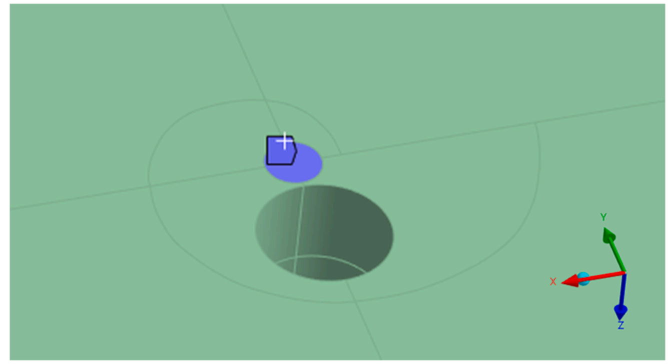

Fig. 8. In blue the area of the fixed support at the mirror back-surface centre, close to the water inlet hole: the nodes included have all the degrees of freedom fixed.

4. Results

The results analysed in this section are mainly the temperature and the deformation. The maximum or total values will represent the global behaviour, but in this analysis, it is important to evaluate the distribution of the results. The objective is minimizing deformations, keeping the maximum temperature low but also ensuring minimal thermal gradients. The most critical deformation affecting beam propagation in mirrors is the out-of-plane deformation in the Z-direction, which should be analysed independently of the total deformation. Notably, large total deformations do not necessarily correspond to significant Z-directional deformations.

4.1. Transient analysis

The first analysis discussed is the transient analysis, carried out on the flat mirror 02M-L. The main results are reported in Fig. 9.

The trends over time of the maximum temperature (green) and the maximum total deformation (red) of Fig. 9 show visibly that the steady condition is reached well before the end of the shot (110 s), both for thermal and structural results. Although the trends present this attainment only for the maximum values, two factors demonstrate the stability of the conditions when considering the entire distribution of temperature or deformation. First, the plateau is sufficiently long, and second, as shown in Fig. 10, the temperature distribution at 110 s (top) aligns closely with the steady-state distribution (bottom).

Achieving steady-state conditions confirms the possibility of using a less demanding approach, switching to steady-state and static simulations, as follows.

4.2. Thermal and structural results

In this section, the results of the steady-state thermal and static structural simulations for all the mirror models are reported. Fig. 11 shows the contour plots of the temperature distribution on the four models of mirror. The peaks of temperature are registered in the centre of the mirrors, due to the single central reflecting beam. The maximum temperature does not exceed 27.9 °C. The highest value is registered in the first mirror 01M-L, presenting the highest heat flux and absorption coefficients (Table 2). Depending on the thermal load, it happens that the mirror 01M-L has similar results to 02M-S, while 02M-L is similar to

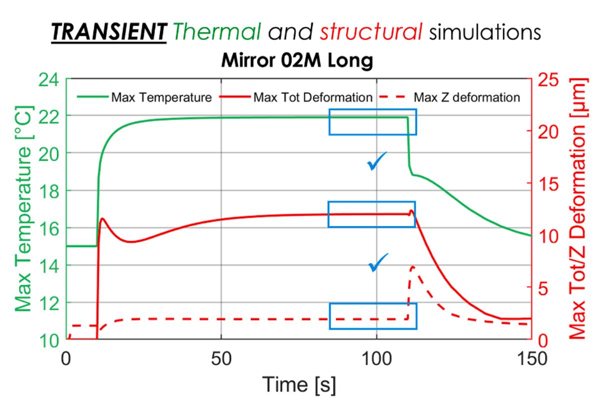

Fig. 9. Graph of the maximum temperature and maximum total deformation over time for the mirror 02M-L.

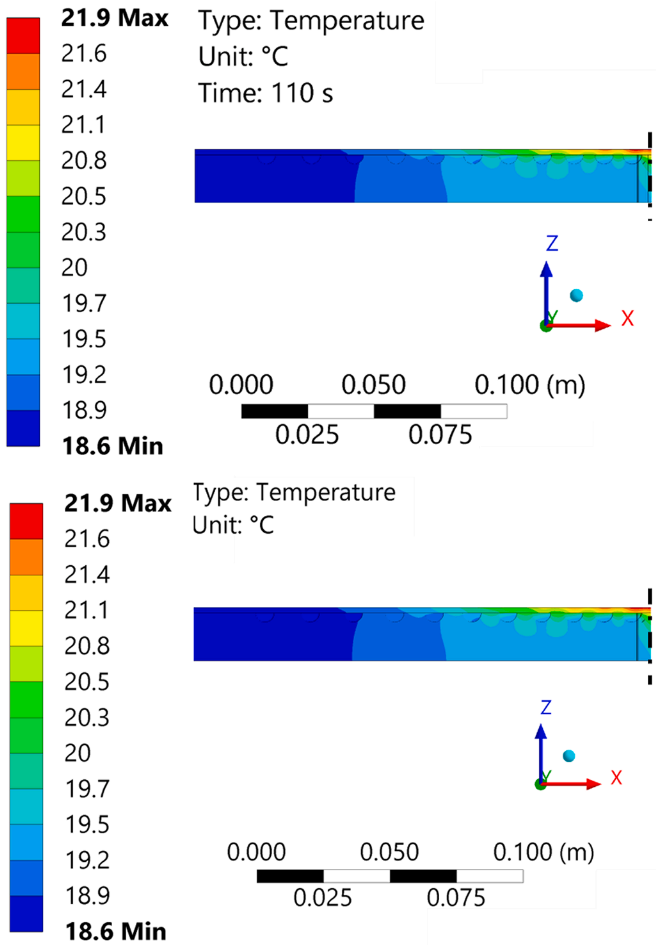

Fig. 10. Contour plot of the temperature on a portion of the mirror 02M-L, x-z section view, at 110 s (top) and in steady-state (bottom).

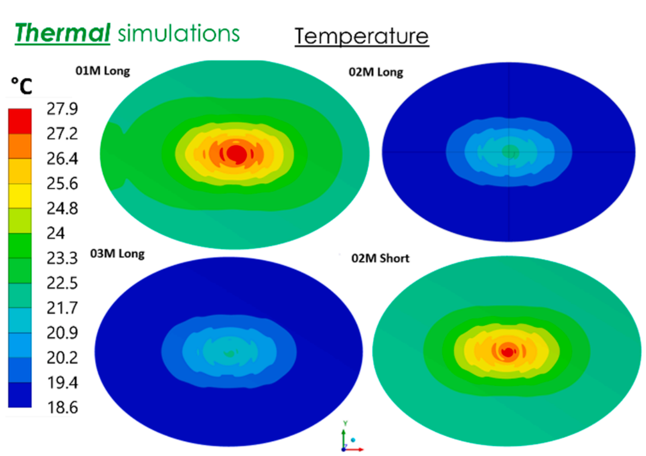

Fig. 11. Contour plots of the temperature distribution of the four mirror models.

03M-L. Referring also to Table 3, reporting the maximum and minimum values of the temperature, it is noteworthy that the maximum differences temperature are small: respectively (6; 3.3; 3.1; 5.8) °C and much smaller are the estimations of the maximum thermal gradients: (0.10; 0.06; 0.06; 0.11) °C/mm. The water outlet temperature, shown in Table 3, varies for each mirror due to the different amounts of heat to be dissipated. In fact, for a constant flow rate, the outlet temperature in steady state is directly proportional to the heat, as described by the equation $Q = mc_p\Delta T$.

Table 3
Maximum and minimum temperatures and water outlet temperatures for the four mirror models.

Mirror model	Max Mirror Temp.	Min Mirror Temp.	Water Outlet Temp.
01 M L-Line	27.9 °C	21.9 °C	22.2 °C
02 M L-Line	21.9 °C	18.6 °C	18.8 °C
03 M L-Line	21.7 °C	18.6 °C	18.8 °C
02 M S-Line	27.3 °C	21.5 °C	21.8 °C

Fig. 12 shows the contour plots of the total deformation of the four mirror models. The maximum value is 23 µm. The peaks of deformation are registered in the mirrors with the highest temperature gradients (01M-L and 02M-S). The location of the peaks is on the edges of the major axis (dashed in black on 02M-S). Table 4 shows the values of the maximum total deformation and the maximum/minimum Z directional deformation. It is worth noting that the extreme values (max and min) of the Z directional deformations are very low, not higher/smaller than 3.45 µm and −4.79 µm (15 % and 21 % of the correspondent max total deformation).

The graph in Fig. 13 shows the Z deformations on the long axis for all the models. Here it can be appreciated the shape of the deformation, convex in the negative Z direction. In this plot, it is noticeable the effect of deformation due to the pressure inside the channel on a thin layer of 2 mm, whose consequences on the beam have still to be analysed.

These results are very interesting for ensuring low transmission losses in reflection of the beams. Indeed, the magnitude of the obtained results would not seem to raise concerns regarding the assessment of beam degradation during propagation in case of deformed mirrors. However, such results shall be verified with electromagnetic analyses.

4.3. Thickness parametric analysis

In order to assess how mirror thickness may affect the surface deformation of this type of mirror, a parametric analysis is carried out for the 01M-L mirror. The scope is evaluating if the chosen thickness of 20 mm is a reliable solution. Considering a fixed minimum layer thickness of 2 mm, different total thicknesses are studied: 15, 20, 25 and 30 mm.

From a thermal point of view, the change in thickness does not affect the temperature, being the heat flux and the cooling condition unaffected. Concerning the deformation, the results are reported in Table 5: the maximum total deformation decreases by 10 % passing from 15 mm to 30 mm. The advantage in the total deformation is given by the great improvement in the minimum Z directional deformation, which is reduced to 0.26 µm. As opposed, the maximum Z directional

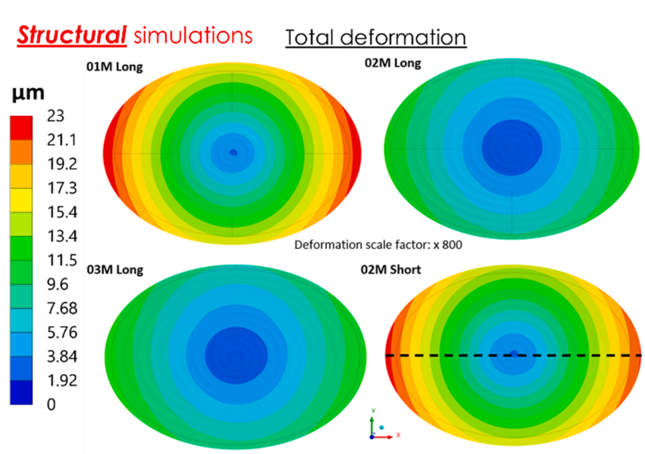

Fig. 12. Contour plots illustrating the total deformation for the four mirror models. Scale factor: x 800.

Table 4
Maximum total deformation and maximum/minimum Z directional deformation of the four mirror models.

Mirror model	Max Tot. Def. Mirror	Max Z Def. On reflecting surface	Min Z Def.
01 M L-Line	23.0 μm	3.45 μm	−4.79 μm
02 M L-Line	12.0 μm	1.94 μm	−3.35 μm
03 M L-Line	12.5 μm	1.95 μm	−3.88 μm
02 M S-Line	22.3 μm	3.32 μm	−4.65 μm

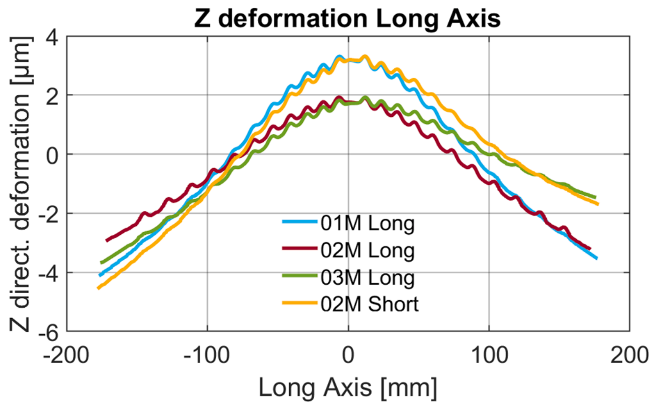

Fig. 13. Comparison of Z-directional deformation trends along the long axis for the four mirror models.

Table 5
Deformation results of the parametric analysis on the thickness.

Total Thickness	15mm	20mm	25mm	30mm
Tot DEF [μm] Mirror	24.9	23.0	22.5	22.3
Z DEF Max [μm] On reflecting surface	2.83	3.45	4.10	4.73
Z DEF Min [μm] On reflecting surface	−9.93	−4.79	−1.76	0.26

deformation increases to 4.73 μm.

Fig. 14 reports the trends of the Z directional deformation of the long axis for the four configurations of thickness, in which the configuration 30 mm appears as the best, despite the highest maximum Z deformation (in the centre).

As shown in Table 5, the maximum Z-deformation does not decrease with increasing thickness. To better highlight the improvements associated with increased thickness, the differences between the maximum and minimum Z-deformations are plotted in Fig. 15. While the maximum values increase with thickness, the minimum values decrease significantly more, resulting in a reduction of the ΔZ deformation by 60 % and 40 % for the 15/30 mm and 20/30 mm configurations, respectively.

However, the initial assumption of 20 mm appears to be a reasonable choice. Nevertheless, the final configuration will undergo further evaluation based on the results of electromagnetic analyses.

5. Conclusions

The design of 4 SBG mirrors was presented. The geometry was defined considering the shape, the curvature of the reflecting surface and the cooling circuit (a single spiral with variable pitch to concentrate the cooling near the heat flux peak). A structured and fine mesh was properly generated to ensure consistency and accuracy of the results. The transient thermo-structural analysis on the mirror 02M-L confirmed the achievement of the steady condition well before 100 s, ensuring the possibility to analyse the other mirrors in steady and static conditions. The mirror 01M-L, with the highest peak of absorbed power, reaches the

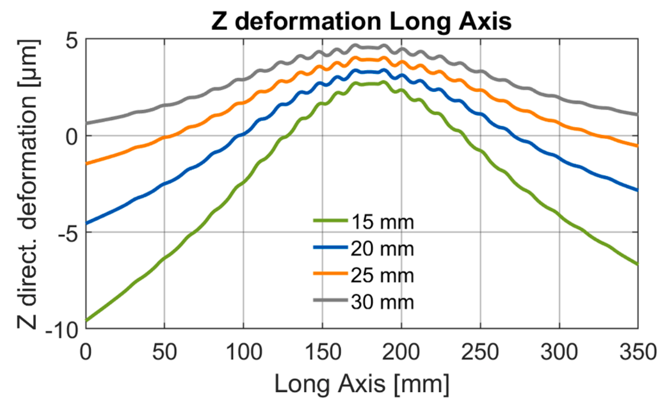

Fig. 14. Comparison of the Z directional deformation of the long axis for the four examined thickness values.

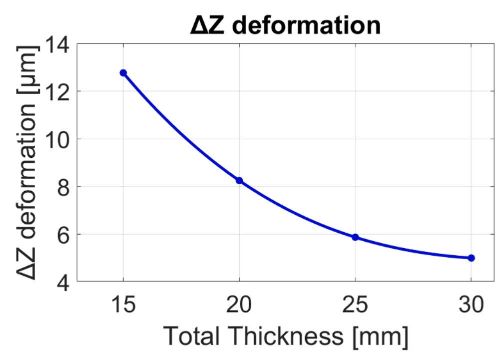

Fig. 15. Trend of the maximum ΔZ deformations for the four examined thickness values.

highest maximum temperature (~28 °C) and consequently the highest maximum total deformation (23 μm). The relative Z-directional deformation, more relevant for the beam deformation after reflection, is ~ 5 μm. Finally, a parametric analysis of the thickness indicates a reduction in deformations with increased thickness. However, given the consistently low values obtained in configuration 2 cm, it seems a good solution, even if the final choice needs further evaluations based on the electromagnetic analysis. In the end, the global results seem very promising for the optical analysis, to ensure minimal transmission losses in reflection of the beams in case of deformed SB mirrors.

CRediT authorship contribution statement

A. Salvitti: Writing – review & editing, Writing – original draft, Visualization, Software, Methodology, Formal analysis, Data curation, Conceptualization. **A. Moro:** Supervision, Resources, Investigation, Data curation, Conceptualization. **A. Bruschi:** Writing – review & editing, Validation, Supervision, Resources, Conceptualization. **G. Calabrò:** Supervision. **F. Fanale:** Writing – review & editing, Visualization, Resources, Investigation, Conceptualization. **P. Fanelli:** Validation, Supervision, Software, Methodology, Conceptualization. **S. Garavaglia:** Resources. **G. Granucci:** Supervision, Project administration. **S. Meloni:** Writing – review & editing, Writing – original draft, Visualization, Methodology, Formal analysis, Conceptualization. **P. Platania:** Formal analysis. **A. Romano:** Supervision, Project administration.

Declaration of competing interest

The authors declare that they have no known competing financial interests or personal relationships that could have appeared to influence the work reported in this paper.

Acknowledgements

This work is carried out in the frame of the DTT activity. The authors are very grateful to all the colleagues involved in the DTT project for their precious contributions.

Data availability

Data will be made available on request.

References

[1] F. Romanelli, et al., Divertor Tokamak Test facility Project: status of design and implementation, Nucl. Fusion 64 (2024) 112015, https://doi.org/10.1088/1741-4326/ad5740.
[2] G. Federici, et al., Demo design activity in Europe: progress and updates, Fusion Eng. Des. 136 (2018) 729–741, https://doi.org/10.1016/j.fusengdes.2018.04.001.
[3] S. Garavaglia, et al., Progress of DTT ECRH system design, Fusion Eng. Des. 168 (2021) 112678, https://doi.org/10.1016/j.fusengdes.2021.112678.
[4] S. Garavaglia, et al., Development of the electron cyclotron resonance heating system for Divertor Tokamak Test, J. Vac. Sci. Technol. B 41 (2023) 044201, https://doi.org/10.1116/6.0002396.
[5] G. Granucci, et al., Roles of ECH system in DTT plasma operations, Nucl. Fusion 64 (2024) 126036, https://doi.org/10.1088/1741-4326/ad7742.
[6] A. Romano et al., ECRH system of DTT: an overview and recent achievements, presented at 33rd Symposium on Fusion Technology, SOFT 2024, Dublin, Irland, 2024.
[7] A. Bruschi, et al., Conceptual design of the DTT ECRH quasi-optical transmission line, Fusion Eng. Des. 194 (2023) 113727, https://doi.org/10.1016/j.fusengdes.2023.113727.
[8] S. Garavaglia, et al., Development of the Multi-Beam Transmission line for DTT ECRH system. EPJ Web of Conferences 277, 2023, https://doi.org/10.1051/epjconf/202327704006.
[9] A. Moro, et al., Progress and challenges of the ECH transmission line design for DTT, Fusion Eng. Des. 202 (2024) 114391, https://doi.org/10.1016/j.fusengdes.2024.114391.
[10] F. Fanale, et al., Status of DTT ECH transmission lines and antennae, IEEE Transactions on Plasma Science 529 (2024) 3778–3784, https://doi.org/10.1109/TPS.2024.3382745. Sept.
[11] P.F. Goldsmith, Quasioptical Systems, Wiley-IEEE Press Springer US, 1998.
[12] L. Empacher, et al., Analysis of a multiple-beam waveguide for free-space transmission of microwaves, IEEE Trans. Antennas Propag. 49 (3) (2001) 483–493, https://doi.org/10.1109/8.918625.
[13] V. Erckmann, et al., ECRH for W7-X: transmission losses of high-power 140-GHz wave beams, Fusion Sci. Technol. 55 (1) (2009) 16–22, https://doi.org/10.13182/FST09-A4049.
[14] A. Salvitti, et al., Preliminary thermal and structural analyses on the parabolic mirror of the Multi-Beam Transmission Line of the DTT ECH system, Fusion Eng. Des. 200 (2024) 114106, https://doi.org/10.1016/j.fusengdes.2023.114106.
[15] A. Salvitti, et al., Thermal and structural analyses on different mirrors of the Multi-Beam Transmission Line of DTT ECH system, Fusion Eng. Des. 201 (2024) 114228, https://doi.org/10.1016/j.fusengdes.2024.114228.
[16] GRASP, Technical description, TICRA. Knud Pontoppidan, 2017. https://www.ticra.com.
[17] V. Erckmann, et al., Electron cyclotron heating for W7-X: physics and technology, Fusion Sci. Technol. 52 (2) (2007) 291–312, https://doi.org/10.13182/FST07-A1508.
[18] W. Kasparek, et al., Mirror development for the 140 GHz ECRH transmission system on the stellarator W7-X, Fusion Eng. Des. 53 (1–4) (2001) 545–551, https://doi.org/10.1016/S0920-3796(00)00532-9.
[19] H. Hailer, et al., Mirror development for the 140 GHz ECRH system of the stellarator W7-X, Fusion Eng. Des. 66 (2003) 639–644, https://doi.org/10.1016/S0920-3796(03)00264-3.
[20] ANSA, Pre-Processor, ANSA version 22.1.x User Guide, 1990-2022 BETA CAE SYSTEMS, updated in April 2022, (https://www.beta-cae.com/ansa.htm).
[21] A. Salvitti, et al., Preliminary design and thermal analyses of the steerable mirror cooling channel of the DTT ECRH, Fusion Eng. Des. 161 (2020) 111880, https://doi.org/10.1016/j.fusengdes.2020.111880.
[22] A. Allio, et al., Assessment of the performance of different cooling configurations for the launcher mirrors of the ECRH system of the DTT facility, IEEE Trans. Plasma Sci. 50 (11) (2022) 4054–40591, https://doi.org/10.1109/TPS.2022.3182532.